SPECTROSCOPIC OBSERVATIONS OF IMPURITIES IN TOKAPOLE II DISCHARGES

R.J. Groebner
J.C. Sprott
R.N. Dexter

PLP 796

May 1979

Plasma Studies

University of Wisconsin

SPECTROSCOPIC OBSERVATIONS OF IMPURITIES IN TOKAPOLE II DISCHARGES

R.J. Groebner, J.C. Sprott, R.N. Dexter
University of Wisconsin Physics Department
Madison, Wisconsin 53706

ABSTRACT. Tokapole II is a tokamak with a four-node poloidal divertor. Impurity concentrations, line radiated power, and impurity behavior have been studied in Tokapole II discharges with two VUV spectrometers, one of which acquires the VUV spectrum (400-1300 Å) with a single discharge. Oxygen (3-5% of the electron density) is the dominant impurity, and the measured total radiated power is 15-30% of the ohmic input power. Observed metal impurities cannot be generated by sputtering from the 15-20 eV plasma protons; sheath potentials evidently play a dominant role in the generation of the metal impurities. An impurity doping technique has been used to measure the impurity concentrations, to estimate the contributions of the various low-Z impurities to the total radiated power, and to study the gross effects of impurities on the plasma. A model of impurity behavior in a plasma with a magnetic limiter is presented.

SPECTROSCOPIC OBSERVATIONS OF IMPURITIES IN TOKAPOLE II DISCHARGES

R.J. Groebner
J.C. Sprott
R.N. Dexter

C00-2387-108

May 1979

1. Introduction

Impurities strongly influence tokamak plasmas. Impurity line radiation accounts for 10-60% of the power loss in tokamaks [1-5]. Multiply-charged impurity ions typically increase the plasma resistivity by factors of 2 to 10 [2-6]. Impurities (primarily low-Z) are strongly implicated in the onset of the disruptive instability [7]. When the low-Z impurity concentration is reduced, the edge temperature rises, leading to an increased production rate of high-Z impurities, which can produce hollow electron temperature profiles in unfavorable cases [8].

Magnetic divertors are being used in several machines [9-12] to control impurities. The impurity problems in tokamaks with magnetic divertors may differ from those in conventional tokamaks. This paper describes initial studies of impurity behavior in discharges in Tokapole II, a tokamak with a four-node poloidal magnetic divertor. The primary diagnostics for these studies were two vacuum ultraviolet (VUV) spectrometers, one of which surveys the 400-1300 Å region of the VUV spectrum during a single discharge. The survey instrument is described, quantitative impurity measurements are presented, and a model of the oxygen impurity behavior is discussed. Results of impurity doping experiments and an interpretation of impurity behavior in the magnetic limiter configuration are emphasized.

2. Description of Machine and Discharge

Tokapole II, first operational in April, 1978, has been described in detail elsewhere [13]. The aluminum vacuum vessel has a major radius of 50 cm and a square minor cross section which is 44 cm on a side. Four

internal rings, fabricated from an alloy of copper and chromium, are each supported by three Cu-Be rods. Figure 1, obtained from an MHD equilibrium code which models Tokapole plasmas, shows the cross section of the toroid and the poloidal magnetic field flux plot with currents in the plasma and in the rings. Also shown is a retractable baffle plate which can be inserted between one of the internal rings and the wall.

An iron core transformer inductively drives the ring and plasma currents. The plasma current produces a set of nested, closed flux surfaces with square cross sections in the region between the rings. As is shown in Fig. 1, a separatrix surrounds the central current channel and each of the internal rings, and thus a magnetic limiter is established.

Figure 2a shows the timing of the fields. When the toroidal field has been established, ECRH preionization is used to produce a low density plasma in 3×10^{-4} Torr of H_2. Current is then induced in the plasma and in the rings. As a function of time, the poloidal gap voltage is a cosine with a quarter period of 2.8 msec. Figure 2b shows the temporal development of the plasma current I_p and the line-averaged electron density $\overline{n_e}$. In the work to be discussed, I_p was about 40 kA and $\overline{n_e}$, measured with a microwave interferometer, was about $7\text{-}8 \times 10^{12}$ cm^{-3}. Figure 3 shows the ion and electron temperatures as functions of time. The ion temperature T_i was roughly constant at about 17 eV and the electron temperature T_e reached about 100 eV at 1.5 msec, and it probably rose no higher. The T_e measurement will be discussed in section 5. These results are preliminary measurements made at magnetic field strengths and pulse lengths well below the design limits of the device.

3. Diagnostics

Spectroscopic observations in the 2000-6500 Å range were made with a ½-meter Jarrell-Ash monochromator equipped with an EMI 9635 QB photomultiplier

tube. Observations in the vacuum ultraviolet (VUV) region (400-1600Å) were made with a 1-m Seya-Namioka monochromator which was equipped with a photomultiplier tube behind a sodium salicylate-coated window and also with a windowless electron multiplier. A mirror on a bellows was used to direct the beam to the desired detector. In addition, a ½-m Seya spectrometer, with a gold-plated grating and with a microchannel plate in its exit plane, was used to survey the spectrum from 400-1300 Å on one shot.

Prior to its use on Tokapole II, the 1-m Seya had been relatively calibrated while attached to the synchrotron radiation source at the University of Wisconsin Physical Sciences Laboratory. Although this source is linearly polarized and plasma light is unpolarized, it was assumed that the relative calibration described the gross features of the monochromator response to plasma radiation. An absolute calibration was performed with rare gas resonance microwave discharge lamps [14] and a four-plate ionization chamber [15], which was used to measure the photon flux from the lamps. The relative calibration was then scaled to fit the calibration points. The accuracy of the absolute calibrations is estimated to be about 25% and that of the overall calibration to be within a factor of two.

The ½-m survey system is illustrated schematically in Fig. 4. VUV photons are converted to electrons in the microchannel plate. This electron current is multiplied and then converted into visible photons by a phosphor screen. Thus, spectral lines in the VUV are made visible and can be photographed to give a picture of all lines present during a discharge or can be viewed by a Quantex gated storage vidicon and displayed on a TV screen. This latter capability permits the recording of the VUV spectrum from a selected time interval (as short as 10 μsec) during the discharge. With the gated vidicon the temporal evolution of the VUV spectrum (400-1300 Å) can be obtained with a small number of discharges.

The anode current of the microchannel plate is produced by photons which have energies larger than about 8 eV; this current is roughly proportional to the total flux of photons entering the Seya, and in turn this flux is roughly proportional to the total radiated power. The anode current will be called the integral VUV or the VUV signal, and this signal was calibrated in terms of radiated power from a comparison of its value during a specific type of discharge to the total radiated power of that discharge as measured by the 1-m Seya. The VUV signal is very useful for noting relative changes of radiated power from one discharge to the next. The absolute calibration is subject to compounded errors of perhaps 50%.

A detector which consists of a polypropylene filter and a channeltron was used to make relative measurements of power radiated in the soft x-ray (SXR) region (60-300 eV). Other broadband filters with appropriate detectors were used to provide additional information in the visible and VUV regions. These broadband detectors and the SXR detector were placed in swivel ports, and they provided spatial information on impurity radiation.

4. Impurity Measurements

4.1 Impurity Identification and Radiated power

Locating and identifying impurity lines produced in a discharge were greatly facilitated with the aid of spectra from the 1/2-m Seya. Nearly all of the observed lines were attributed to oxygen, carbon, nitrogen, and copper. In addition, resonance lines of the lower ionization states of aluminum, chromium, and beryllium were identified in the near UV and visible.

Quantitative spectroscopic measurements were made with the 1-m Seya by the techniques discussed in Ref. 2. The formulae therein were modified for the square symmetry of Tokapole II. Measurements of the dirty discharges during the initial phase of machine operation indicated that about 290 kW of

power was being radiated (about 70% due to carbon) while the input power was about 390 kW. At that time the VUV integral detector was calibrated, and it has been used routinely since then to measure the radiated power. Discharge cleaning greatly reduced the plasma impurity content to the point that in typical discharges, the radiated power loss of about 35 to 70 kW was not more than 15 to 30% of the ohmic input power.

4.2 Impurity Doping Results

To more fully assess the role of impurities in Tokapole II discharges, a phenomenological study was performed in which controlled amounts of O_2, N_2, and CH_4 were introduced with a fast-acting valve into the vacuum chamber prior to the initiation of the discharge, and the behavior of selected parameters was observed. In a manner similar to that used by Oren and Taylor to measure the amount of the oxygen contamination on a tokamak wall [16], the technique used here provided a convenient method for determining the densities of the low-Z impurities early in the discharge. Figure 5 illustrates this technique for oxygen. The intensities of the ionization peaks of bright lines of OIII-OVI are plotted as functions of the O_2 doping concentration. With the possible exception of the OV data, the extrapolation of the data points for each ion to zero intensity corresponds to an O_2 concentration of 1.6×10^{11} cm^{-3} (3.2×10^{11} cm^{-3} of atomic oxygen). These data indicate that the oxygen concentration early in the undoped discharge was 3.2×10^{11} cm^{-3}. Since the filling density of H_2 was 5×10^{12} cm^{-3}, oxygen was a 3% impurity in this case.

The doping data consistently indicated that the initial oxygen concentration in Tokapole plasmas was 3-5% of that of the electrons. The carbon density was

typically about 5×10^{10} cm^{-3} (0.5%). When an air leak resulting in a base pressure of $1\text{-}2 \times 10^{-7}$ Torr was present, the plasma nitrogen density was $2\text{-}4 \times 10^{11}$ cm^{-3}. No measurements of the metal concentrations were made.

Figure 6 is a plot of the intensity of the ionization peak of OIV λ790 Å (OIV 790) vs. the maximum VUV signal (VUV_M) during an oxygen doping sequence. (The VUV signal was relatively constant during the discharge and is well represented by VUV_M). By the same reasoning used previously, the data points can be extrapolated to the VUV axis to find what percentage of the VUV signal was attributable to oxygen. In this case, the oxygen contribution was about 25%; typically, it was between 25 and 35%. When a full set of data was obtained, carbon accounted for about 5% of the VUV, oxygen for about 30%, nitrogen for about 25%, and almost 40% was not accounted for. Presumably, this latter portion of the VUV radiation was produced by metals. More recent VUV spectra show fewer metal lines than observed previously, and a repeat of the doping experiments has shown that 85% of the VUV signal can be attributed to oxygen, carbon, and nitrogen.

The integral of plasma current over time (called amp-seconds or AS) is a convenient parameter which is used to indicate the "quality" of the discharge. Dirty, low-temperature discharges are characterized by low values of AS (as low as 25). Clean, high temperature discharges last longer than the dirty discharges and are characterized by values of AS of 100-130. Figure 7, which is a plot of AS vs. the VUV_M signal (or equivalently the radiated power) during an oxygen doping run, shows that for low values of the radiated power P_{rad}, AS was independent of P_{rad}, and at higher values of the radiated power AS decreased linearly with P_{rad}. Similar observations were made with N_2 and CH_4 doping.

In Fig. 8, AS has been plotted against the peak SXR signal SXR_M. With no doping, AS was 98 while SXR_M was 80. With increasing doping concentrations, the AS level remained constant, which is interpreted to mean that the electron temperature was not changing. Also, the SXR signal increased because there was more oxygen available to radiate. Eventually a level of doping was reached at which AS started to drop and the SXR signal remained roughly constant. The fall in AS evidently corresponded to a cooling of the plasma. As the doping level increased, oscillations in the SXR signal increased in amplitude. MHD activity associated with these oscillations in combination with impurity radiation probably cooled the plasma.

4.3 Impurity Sources

Several observations indicate that early in the discharge, the impurities are evolved primarily from the vacuum chamber walls and that after the current channel is well formed, the impurities are evolved primarily from the rings. Electrical probe measurements have shown that at early times the current and electron densities are peaked near the walls; the central current channel is well established by about 1.2 msec, and only then does the electron temperature start to rise rapidly. The hot plasma is then confined mainly to the region within the magnetic limiter, and the most intense plasma-surface interaction is expected to occur at the rings. Insertion of the retractable baffle plate into the plasma between the wall and one of the rings (Fig. 1) reduced the VUV signal during the first millisecond of the discharge as compared to the VUV signal observed without the baffle; at later times, the integral VUV signals were quite similar with or without the baffle. The

baffle, which reduced the plasma density outside the separatrix, effectively reduced the severity of the plasma-wall interaction; but at best, the baffle could only reduce plasma bombardment at one of the rings, and the others were not shielded.

Metal production in Tokapole discharges apparently requires the presence of sheath potential effects. The protons are not sufficiently energetic to produce significant sputtering; nonetheless, metal impurity lines are observed, copper from the rings has been spread around the machine, and the vacuum surfaces show much evidence of arcing and sputtering. As has been discussed elsewhere [17-19], sheath potentials at metal-plasma interfaces are required for the formation of unipolar arcs, which can inject metal into the plasma, and these potentials can also accelerate plasma ions to energies considerably larger than their thermal energies and thus greatly increase the sputtering yield of the ions.

The sheath potentials in Tokapole II plasmas have not been directly measured. Measurements of the floating potential with a probe in the scrape-off region, of the ring potentials, and of T_e suggest that the sheath potentials are less than or of the order of 100 eV; presumably, such potentials could produce unipolar arcs. Furthermore, an ion of charge Z falling through a sheath potential of V volts would acquire an additional energy of Z eV, where e is the electronic charge, so that multiply-charged impurity ions falling through a sheath potential which was less than or equal to 100 V could have energies of up to a few hundred eV. Such ions have significant sputtering yields and could account for metal production in Tokapole discharges. A preliminary experiment has shown that the copper production rate can be reduced when the rings are biased positively with respect to the vacuum chamber walls.

5. Oxygen Modeling

To provide insight into the oxygen ion behavior and to form an estimate of the electron temperature, a time dependent coronal calculation was used to model the ionization of the oxygen ions [2].

Figure 9 shows the observed evolution of resonance lines of OIII - OVI. The ionization peaks were enhanced with the addition of 3.5×10^{11} cm^{-3} of O_2. This did not significantly affect the discharge. The curves in Fig. 9 have been corrected for the relative response of the 1-m Seya.

The following set of rate equations was solved for the densities of the various ions:

$$\frac{dn_o}{dt} = -S_o(T_e)\, n_e\, n_o + \alpha_1(T_e)\, n_e\, n_1 - n_o/\tau + \phi_o$$

$$\frac{dn_z}{dt} = -S_z(T_e)\, n_e\, n_z - \alpha_z(T_e)\, n_e\, n_z + S_{z-1}(T_e)\, n_e\, n_{z-1} + \alpha_{z+1}(T_e)\, n_e\, n_{z+1} - n_z/\tau \quad (1)$$

$$\frac{dn_{zl}}{dt} = -\alpha_{zl}(T_e)\, n_e\, n_{zl} + S_{zl-1}(T_e)\, n_{zl-1}\, n_e - n_{zl}/\tau$$

In these equations, n_o is the atomic oxygen density, n_z is the density of ions of charge Z, n_e is the electron density, τ is the particle confinement time, ϕ is the influx rate of fresh oxygen, which is assumed to be in the atomic state, and zl refers to the limit ion, the most highly charged ion produced in the discharge. S_x and α_z are, respectively, the ionization and recombination rate coefficients for the ion of charge z; they are functions of T_e only. The ionization rate coefficients were taken from Lotz [20], radiative recombination

rate coefficients were taken from Aldrovandi and Péquignot [21], and dielectronic recombination rate coefficients were from Beigman et al. [22]. No attempt was made to correct the dielectronic rates for electron density; since this calculation was for the ionization phase of the impurities, recombination was of very little importance. The emission E of a resonance line was calculated from:

$$E = n_e \, n_z \, Q(T_e) \qquad (2)$$

where $Q(T_e)$ is the electron excitation rate coefficient for the resonance transition under consideration. The excitation rate coefficients were those of Vainshtein et al [23-25].

In circular tokamaks, the impurities are typically uniformly distributed during the ionization phase of the discharge [26]. Available spatial data for impurity radiation in Tokapole II showed that the radiation was primarily emitted from the central current channel. The calculation was performed with the assumption that the impurities were uniformly distributed in the central channel, and the central density was assumed to be 1.35 times the line-averaged density of Fig. 2b.

In the simulation, the input parameters $T_e(t)$, ϕ_o and τ were varied until the computed times of the ionization peaks agreed with the observed times of the peaks. It was found that these times were only weakly dependent on ϕ_o and τ. For the final calculations, ϕ_o was taken as zero since most of the oxygen was present from the beginning, while τ was taken as 3 msec because it gave the best agreement on peak heights.

Figure 10 shows the results of the calculation which provided the best agreement with the observed oxygen ion sequence, and Fig. 3 illustrates the function $T_e(t)$ which was used in this calculation. The electron temperature

remained low while the current was penetrating to the center of the machine, and T_e increased rapidly to about 100 eV after the channel was well established. The SXR signal, which is a strong function of T_e, suggested that T_e peaked between 1.6 and 1.9 msec, and conductivity temperature measurements indicated that T_e decreased relatively slowly after that time.

For the results of the oxygen modeling which have been presented, the densities of the ground states of OIII-OV were corrected for the existence of the metastable levels of those ions [1]. When this correction was not used, the calculated ratio of the peak emission of OV 630 to that of OVI 1034 was about a factor of 3.1 larger than the ratio observed experimentally. With the correction, the calculated ratio is about 77% of the experimentally observed ratio. OIV 789 provides the poorest agreement and this may be due to uncertainties in the correction for the metastables or in the excitation rates.

Figure 9 shows that after its ionization peak, the emission of each ion was relatively constant for the duration of the discharge. This constant emission is generally attributed to an impurity influx [2,26], so an oxygen influx term was included in the computer calculation. Reasonable agreement with the observations was achieved with the assumptions that the influx was OI, that each ion was in a region in which the electron temperature was one-third of its ionization potential (as has been observed in the TFR tokamak [26]), and that the particle confinement time of each ion was 1 msec. Influx calculations in which the influxing oxygen ions were assumed to be at the electron temperature of the central plasma produced very poor agreement with the observations. Without additional information about the T_e and impurity density spatial profiles, the model cannot reasonably be pushed further.

6. Discussion

The measurements and observations presented in this paper represent an initial characterization of the impurity behavior in Tokapole II. The data suggest an interpretation of the behavior of impurities in a plasma with a magnetic limiter, an explanation of the discharge current behavior during impurity doping, and areas of further study, all of which will now be discussed.

A variety of observations suggests that the magnetic limiter configuration works in the following way. A hot central current channel is separated from the cooler (~ 20 eV), but dense ($n_e \sim 2 \times 10^{12}$ cm^{-3}), plasma in the scrape-off region by a separatrix (Fig. 1). The poorly confined plasma of the current build-up phase interacts primarily with the chamber walls and releases impurities to produce the initial impurity concentration. During the steady state phase of the discharge, the primary impurity production probably occurs at the rings, and some of the impurities diffuse into the central current channel.

The scrape-off layer (~10 cm) is expected to insulate the main current channel from the wall. Ions in the scrape-off layer have a large amount of poloidal flux to cross to penetrate to the central channel. Low-Z neutrals released from the wall with energies less than ~3 eV will be ionized and trapped in the magnetic field of the scrape-off plasma. In contrast, neutrals produced at the rings can penetrate into the central channel, or if the impurities are ionized near the rings, they have less poloidal flux to cross to reach the central channel than ions diffusing from the walls. By virtue of its lower temperature and density, the scrape-off plasma has a much less severe interaction with the walls than the hot central plasma would have, and this fact serves to further reduce impurity influx.

Spatial impurity data indicate that the impurity radiation is produced in the central regions of the plasma. The oxygen modeling strongly suggests that the radiation does not come from the hot current channel itself. It is consistent with these observations to assume that the impurity radiation is produced primarily in the vicinity of the separatrix.

The impurity doping studies and preliminary electrical probe measurements of safety factor, current density and toroidal electric field profiles, and of magnetic fluctuations suggest the following interpretation of AS behavior with doping (Figures 7 and 8). At low doping levels, the safety factor q in the vicinity of the magnetic axis drops below one, and internal disruptions prevent the current density from increasing above its q-limited value. The current density profile is unaffected by the low dopant concentrations, so that the total plasma current and thus AS are independent of the doping level.

As the doping level is increased, the oxygen impurity eventually starts to produce a significant increase in the plasma resistivity; this happens primarily because T_e is reduced by the action of impurities and also because the oxygen increases the plasma Z_{eff}. The plasma resistivity increases to the point that the available electric field is no longer sufficient to maintain the original current density. (The ohmic heating power supply is a voltage source.) Therefore, the total current and AS start to drop. With further increases in the oxygen concentration, the plasma resistivity increases, the current density falls, and the AS parameter falls further.

The results and speculations presented in this paper suggest several further areas of study. Additional work is needed to provide a more complete understanding of the mechanisms producing the metal impurities.

Methods to control the plasma-ring interaction, such as ring biasing, limiters, or baffles, could be implemented. Further control of impurities can be attempted by exploiting the magnetic limiter configuration of Tokapole discharges; the use of gettered baffles in the scrape-off region is a logical step in this direction.

Two related areas for study are the effects of impurities in shaping the current density profile and the role of impurities in MHD activity. The use of electrical probes to measure current density and q profiles and to observe magnetic fluctuations in conjunction with impurity doping techniques might permit a study of these problems. Ultimately, such data could unfold the individual roles of ohmic heating and impurity cooling in the shaping of the current density profile.

ACKNOWLEDGEMENTS

The authors gratefully thank M. Mattioli for providing information for some of the electron excitation rate coefficients. We acknowledge helpful discussions with S. Prager. The technical assistance of T. Lovell, R. Vallem, and their maintenance crew has been greatly appreciated. D. Shephard, D. Witherspoon, T. Osborne, B. Lipschultz, M. Phillips, and K. Miller provided valuable data on the electrical and magnetic characteristics of the plasma.

Portions of this paper are based on the Ph.D. thesis of R. Groebner, (University of Wisconsin, 1979).

This work was supported by the United States Department of Energy.

REFERENCES

[1] TERRY, J.L., CHEN, K.I., MOOS, H.W., MARMAR, E.S., Nucl. Fusion 18 (1978) 485.

[2] EQUIPE TFR, Nucl. Fusion 15 (1975) 1053.

[3] BRETZ, N., DIMOCK, D.L., HINNOV, E., MESERVEY, E.B., Nucl. Fusion 15 (1975) 313.

[4] ŌDAJIMA, K., MAEDA, H., SHIHO, M., KIMURA, H., YAMAMOTO, S., et al., Nucl. Fusion 18 (1978) 1337.

[5] BERRY, L.A., BUSH, C.E., CALLEN, J.D., COLCHIN, R.J., DUNLAP, J.L., et al., in Plasma Physics and Controlled Nuclear Fusion Research (Proc. 6th Int. Conf. Berchtesgaden, 1976) Vol. 1, IAEA, Vienna (1977) 49.

[6] EQUIPE TFR, Nucl. Fusion 17 (1977) 1297.

[7] BICKERTON, R.J., Survey of Tokamak Experiments, Culham Laboratory Rep. CLM-R 176 (1977).

[8] HINNOV, E., SUCKEWER, S., BOL, K., HAWRYLUK, R.J., HOSEA, J., MESERVEY, E., Plasma Phys. 20 (1978) 723.

[9] DIVA GROUP, Nucl. Fusion 18 (1978) 1619.

[10] PAUL, J.W.M., AXON, K.B., BURT, J., CRAIG, A.D., ERENTS, S.K., et al., in Plasma Physics and Controlled Nuclear Fusion Research (Proc. 6th Int. Conf. Berchtesgaden, 1976) Vol. 2, IAEA, Vienna (1977) 269.

[11] MEADE, D.M., SINNIS, J.C., in Plasma Wall Interaction (Proc. Int. Symp. Jülich, 1976), Pergamon Press, New York (1977) 683.

[12] HAAS, G., KEILHACKER, M., in Plasma Wall Interaction (Proc. Int. Symp. Jülich, 1976), Pergamon Press, New York (1977) 691.

[13] BIDDLE, A.P., DEXTER, R.N., GROEBNER, R.J., HOLLY, D.J., LIPSCHULTZ, B., PHILLIPS, M.W., PRAGER, S.C., SPROTT, J.C., submitted to Nucl. Fusion.

[14] GORDEN, R., JR., REBBERT, R.E., AUSLOOS, P., Rare Gas Resonance Lamps, N.B.S. Tech. Note 496 (1969).

[15] COLE, B.E., DEXTER, R.N., J. Phys. B 11 (1978) 1011.

[16] OREN, L., TAYLOR, R.J., Nucl. Fusion 17 (1977) 1143.

[17] McCRACKEN, G.M., GOODALL, D.H.J., Nucl. Fusion 18 (1978) 537.

[18] OHASA, K., MAEDA, H. YAMAMOTO, S., NAGAMI, M., OHTSUKA, H., KASAI, S., ODAJIMA, K., KIMURA, H., SENGOKU, S., SHIMOMURA, Y., Nucl. Fusion 18 (1978) 872.

[19] TAYLOR, R.J., OREN, L., Phys. Rev. Lett. 42 (1979) 446.

[20] LOTZ, W., Z. Physik 216 (1968) 241.

[21] ALDROVANDI, S.M.V., PÉQUIGNOT, D., Astron. Astrophys. 25 (1973) 137.

[22] BEIGMAN, I.L., VAINSHTEIN, L.A., VINOGRADOV, A., Sov. Astron. 13 (1970) 775.

[23] VAINSHTEIN, L.A., SOBELMAN, I.I., YUKOV, E.A., Cross Sections for Excitation of Atoms and Ions by Electrons, Nauka, Moscow (1973).

[24] BRETON, C., DE MICHELIS, C., MATTIOLI, M., J. Quant. Spectrosc. Radiat. Transfer 19 (1978) 367.

[25] MATTIOLI, M., private communication.

[26] T.F.R. GROUP, Plasma Phys. 20 (1978) 207.

FIGURE CAPTIONS

Fig. 1. Cross section of toroid with poloidal magnetic field flux plot, produced by ring and plasma currents. Two cm intervals are indicated by marks along the left and bottom borders, and the major axis lies 50 cm to the left of the mid-cylinder. The retractable baffle, with an area of 240 cm^2, can be inserted to intercept the poloidal flux between the upper left ring and the top of the vacuum vessel. The dotted lines indicate the separatrices.

Fig. 2. Figure 2a shows the toroidal magnetic field and the poloidal gap voltage as functions of time. Also shown is the timing of the ECRH preionization pulse. Figure 2b shows the plasma current and line-averaged electron density from a typical discharge.

Fig. 3. Electron and ion temperatures as functions of time. The ion temperature was determined from Doppler broadening measurements.

Fig. 4. The 1/2-meter Seya-Namioka VUV survey instrument, consisting of a concave grating and a microchannel plate, is illustrated. Also shown, schematically, is the gated storage vidicon and its output displayed on a TV screen.

Fig. 5. The brightnesses of selected lines of oxygen are plotted as functions of the oxygen doping concentration. x, OIII 3761. •, OIV 790. Δ, OV 630. o, OVI 1032. Straight lines are least squares fits to the data.

Fig. 6. The brightness of OIV 790 as a function of the VUV signal during an O_2 doping run. With no doping, the VUV signal was 0.10 V. The extrapolation of the straight line, which is a least squares fit to the data, to the VUV axis indicates that the VUV signal would have been decreased by 25% if no oxygen had been present in the plasma.

Fig. 7. The AS parameter (units of ampere-second) as a function of the VUV signal (radiated power) during an oxygen doping run. The horizontal error bar refers to the reproducibility of the VUV signal.

Fig. 8. AS and the peak SXR signal plotted parametrically as functions of the O_2 doping concentration. AS started to drop when the O_2 doping concentration was about 5×10^{11} cm^{-3}. Large amplitude oscillations in the SXR signal were observed at dopant concentrations above 1×10^{12} cm^{-3}.

Fig. 9. The observed temporal evolution of the emission of OIII 703, OIV 789, OV 630, and OVI 1034.

Fig. 10. The temporal evolution of the emission of OIII 703, OIV 789, OV 630, and OVI 1034 as calculated with a time-dependent coronal model. The T_e of Fig. 3 was used in the calculation.

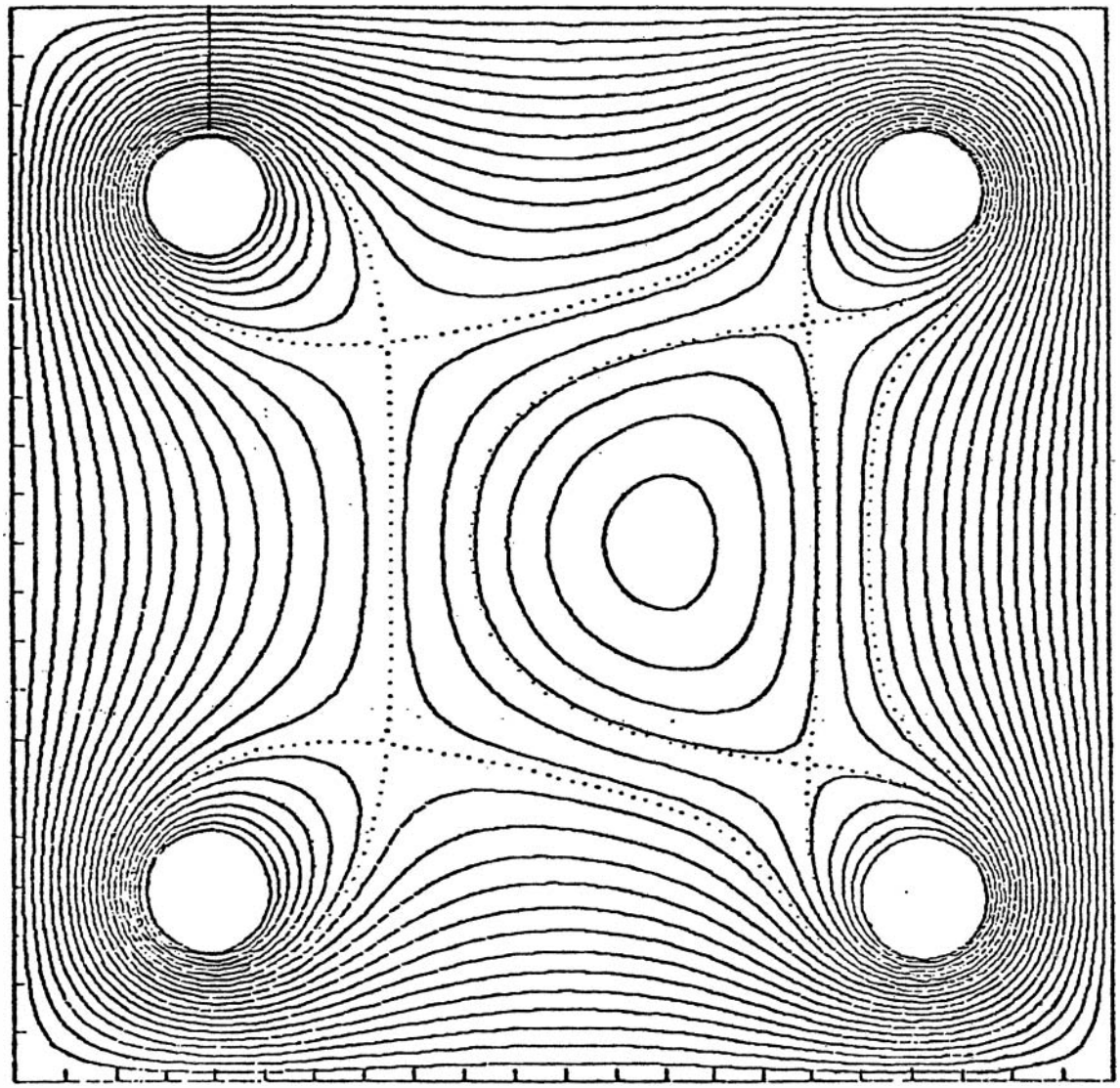

FIG. 1

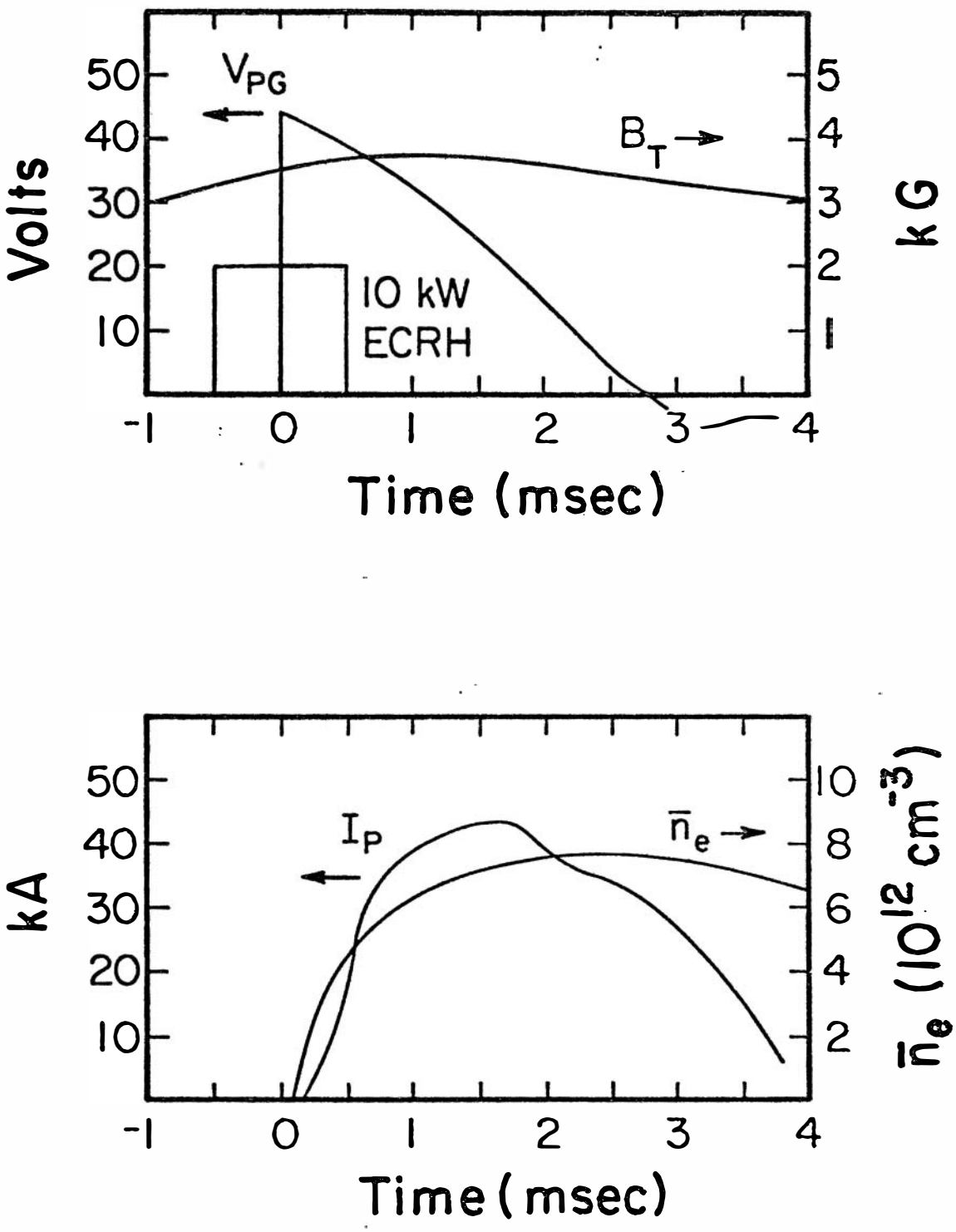
Volts
50
40
30
20
10
V_{PG}
B_T
10 kW
ECRH
5
4
3
2
1
kG
-1
0
1
2
3
4
Time (msec)
kA
50
40
30
20
10
I_P
$\bar{n}_e$
10
8
6
4
2
$\bar{n}_e$ (10^{12} cm^{-3})
-1
0
1
2
3
4
Time (msec)

FIG. 2

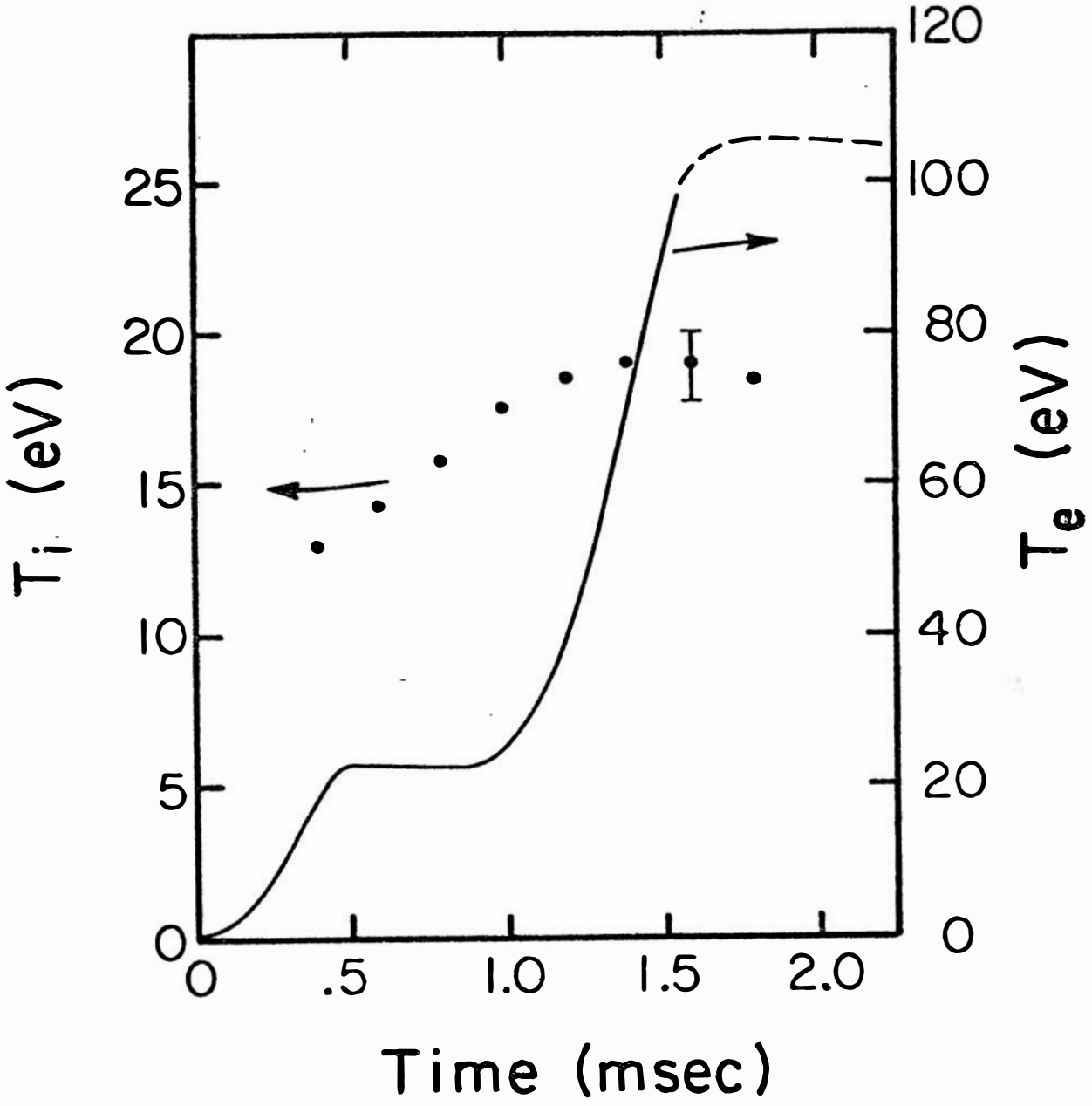

FIG. 3

SCHEMATIC OF VUV SURVEY APPARATUS

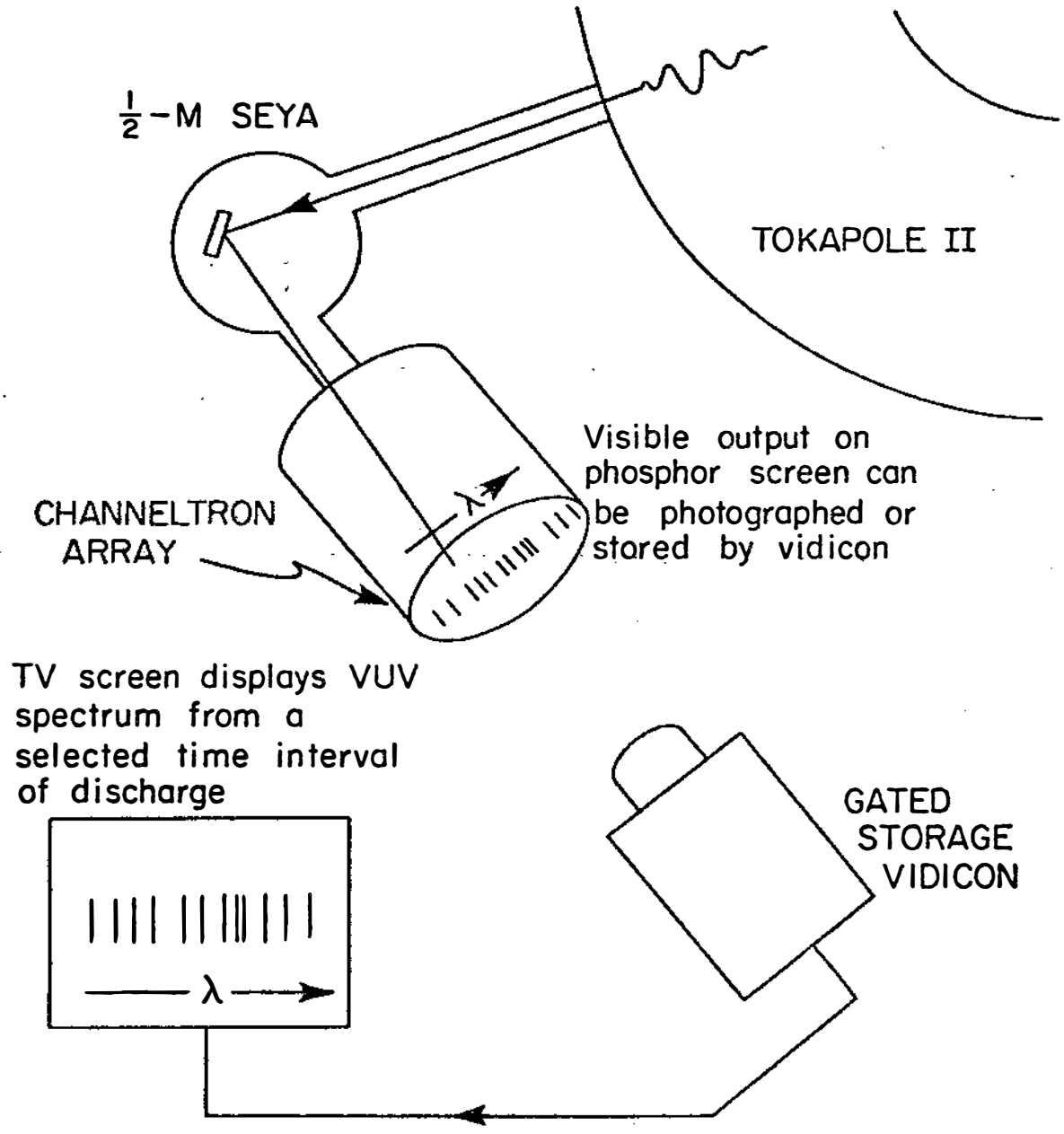

FIG. 4

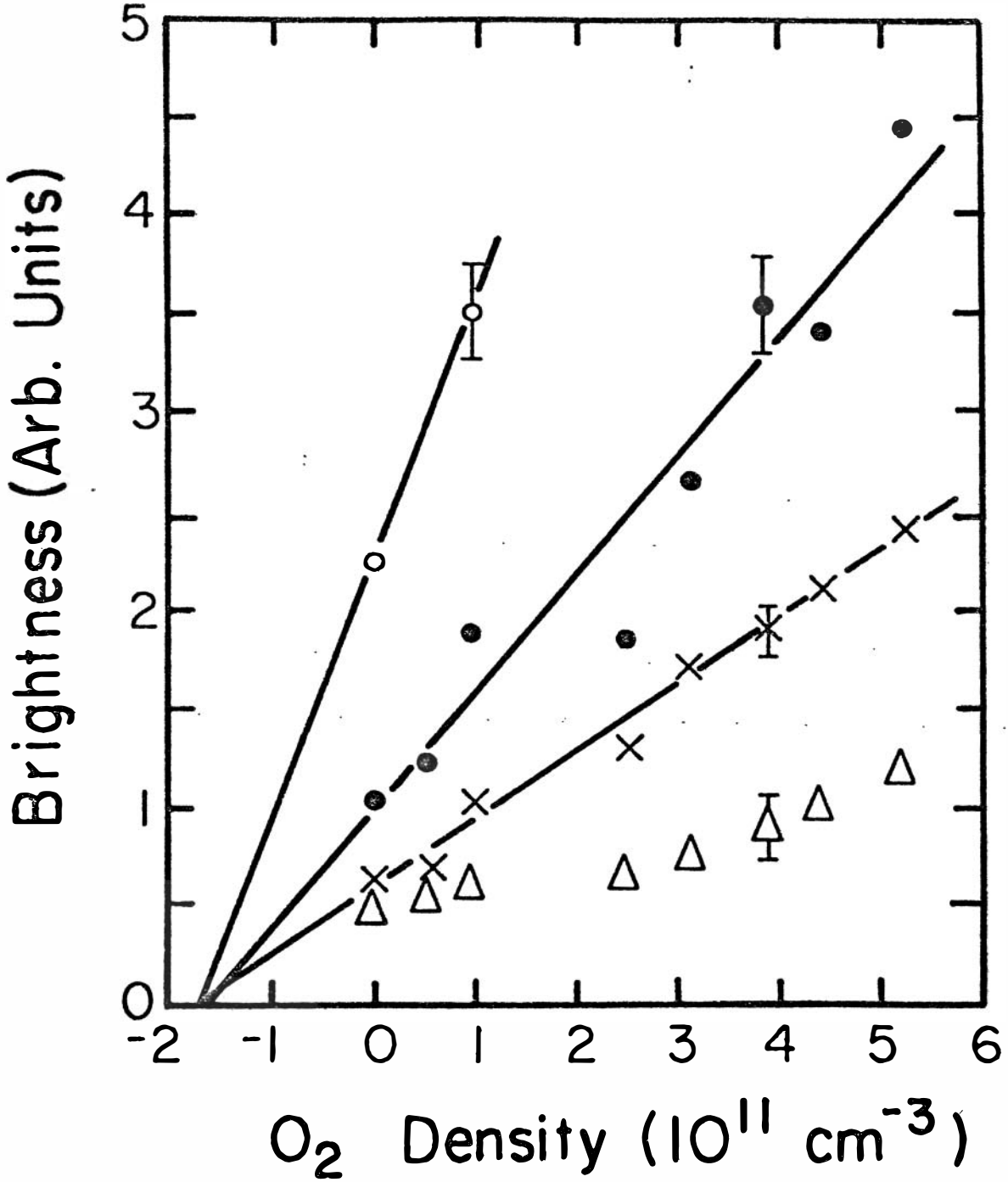

FIG. 5

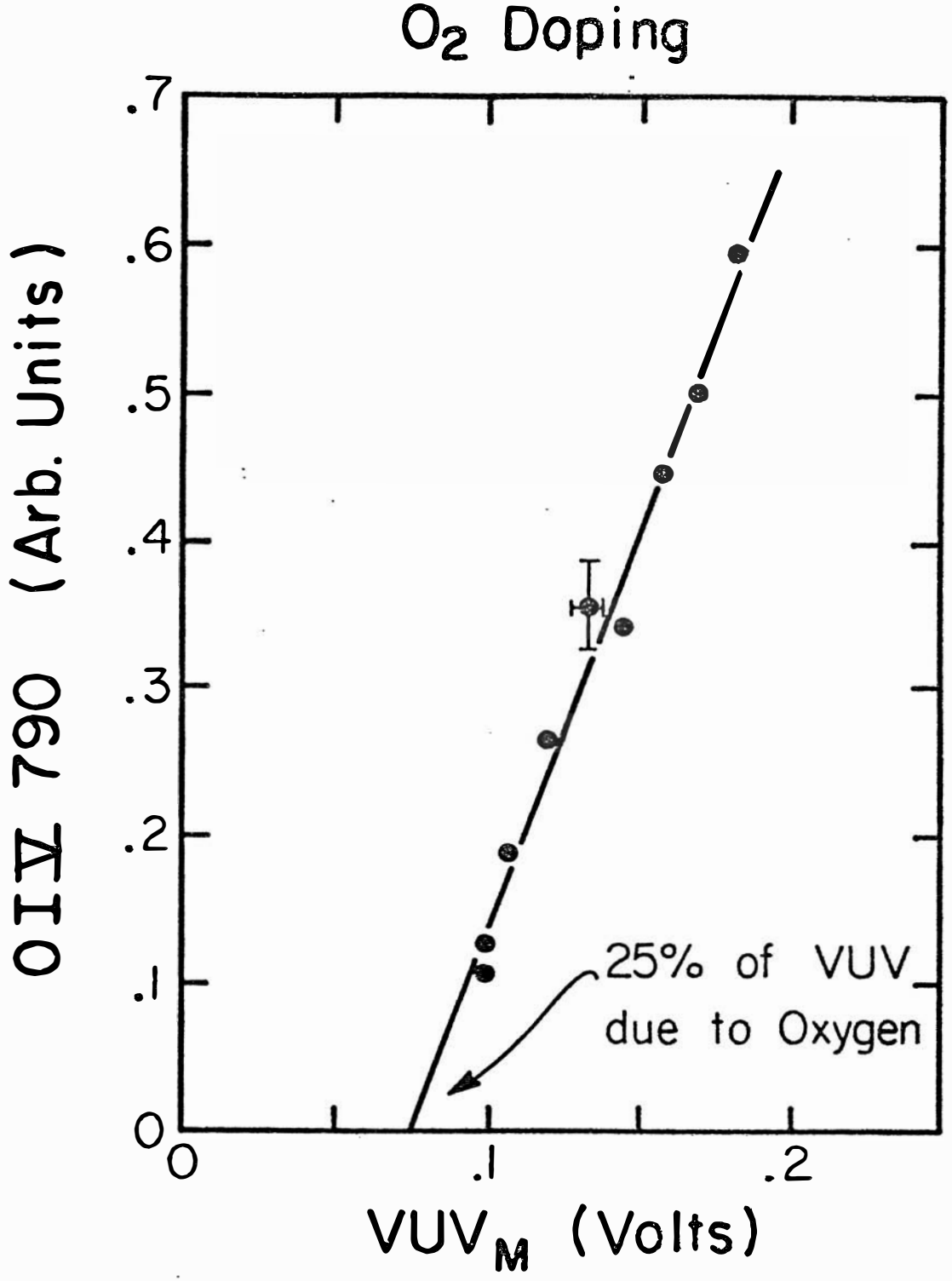
O2 Doping
OIV 790 (Arb. Units)
.7
.6
.5
.4
.3
.2
.1
0
0
.1
.2
VUVM (Volts)
25% of VUV
due to Oxygen

FIG. 6

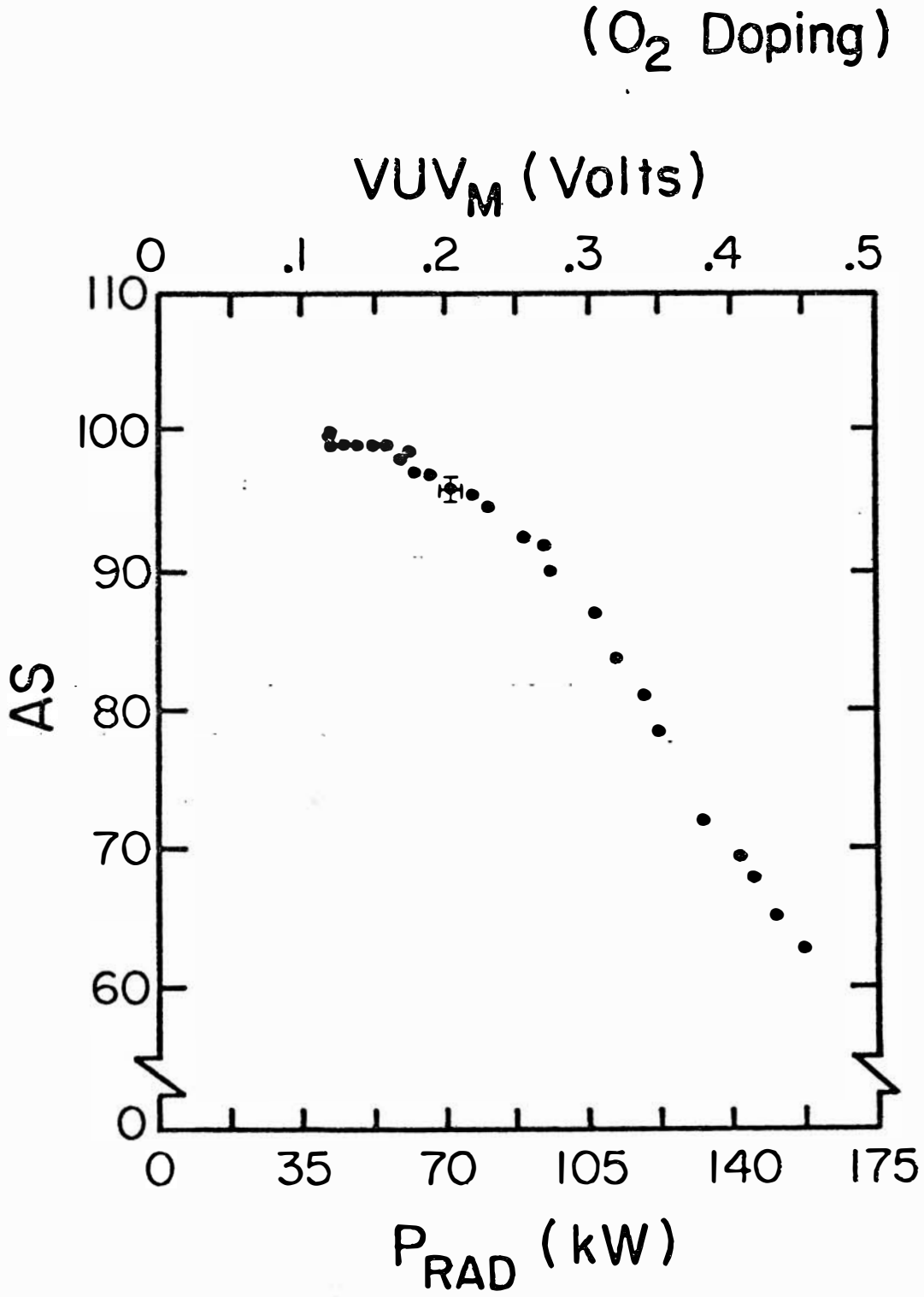
(O_2 Doping)
VUV_M (Volts)
0
.1
.2
.3
.4
.5
110
100
90
80
70
60
0
AS
0
35
70
105
140
175
P_{RAD} (kW)

FIG. 7

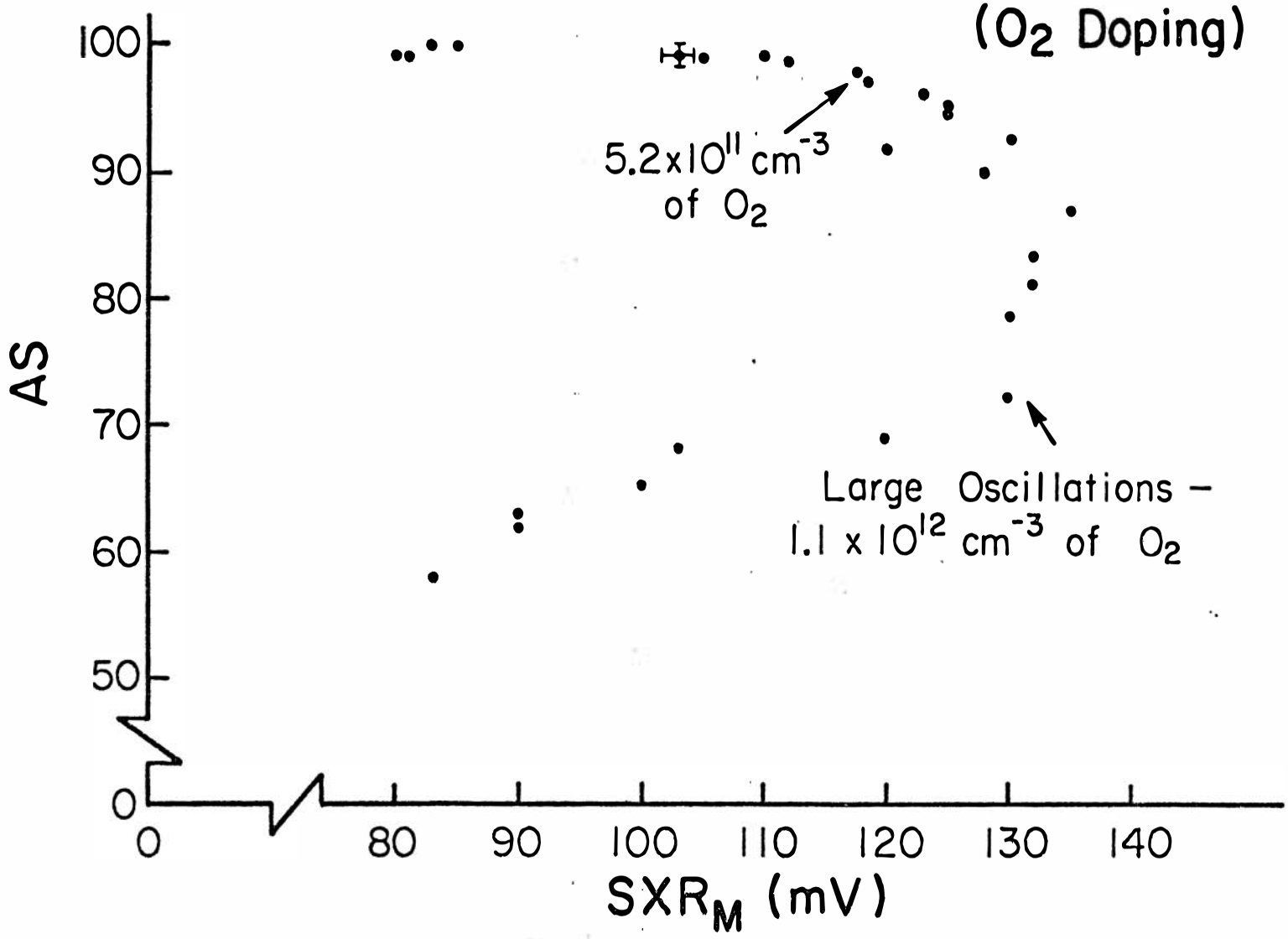
(O2 Doping)
5.2x10^11 cm^-3 of O2
Large Oscillations – 1.1 x 10^12 cm^-3 of O2
AS
SXRM (mV)
100
90
80
70
60
50
0
0
80
90
100
110
120
130
140

FIG. 8

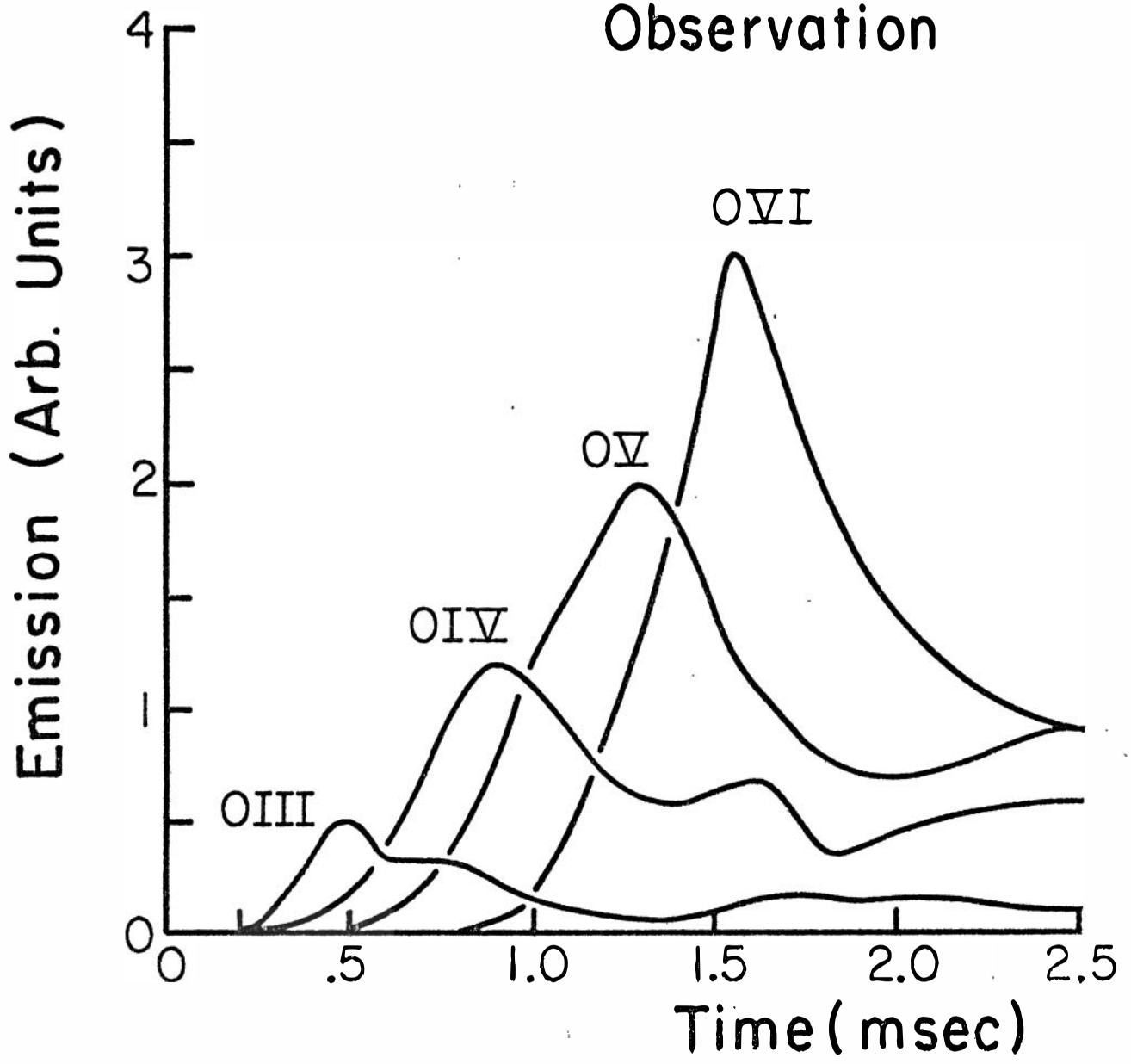
Observation
Emission (Arb. Units)
4
3
2
1
0
0
.5
1.0
1.5
2.0
2.5
Time (msec)
OVI
OV
OIV
OIII

FIG. 9

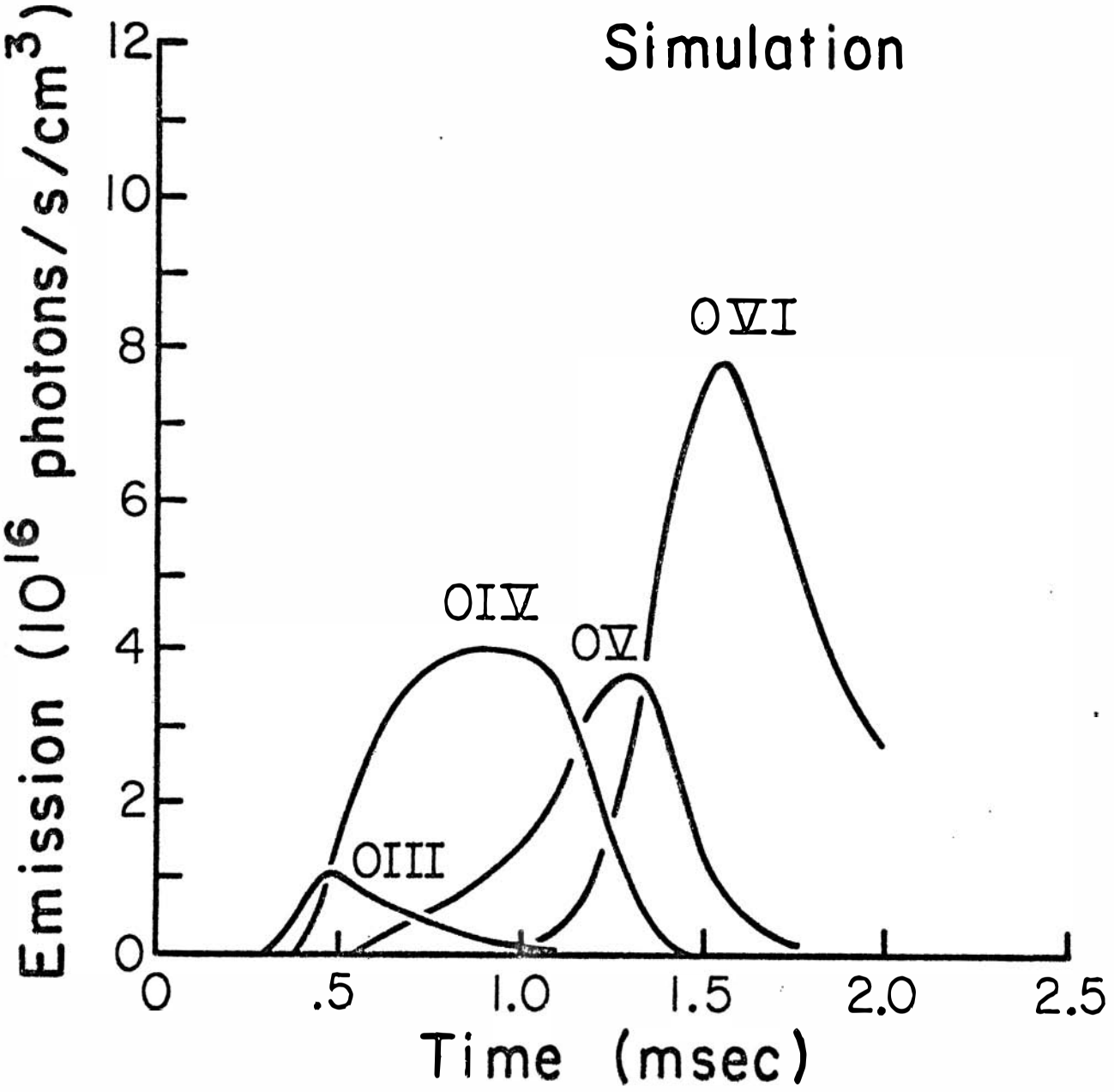
Simulation
Emission (10^{16} photons/s/cm^3)
12
10
8
6
4
2
0
0
.5
1.0
1.5
2.0
2.5
Time (msec)
OVI
OIV
OV
OIII

FIG. 10